


Reynolds number dependence of inner peak turbulence intensity in pipe flow

Cite as: Phys. Fluids **34**, 045103 (2022); <https://doi.org/10.1063/5.0084863>

Submitted: 10 January 2022 • Accepted: 10 March 2022 • Published Online: 04 April 2022

 Marie Ono (小野 満里絵),  Noriyuki Furuichi (古市 紀之), Yuki Wada (和田 裕貴), et al.

COLLECTIONS

 This paper was selected as Featured



View Online



Export Citation



CrossMark

ARTICLES YOU MAY BE INTERESTED IN

[Scaling of rough-wall turbulence in a transitionally rough regime](#)

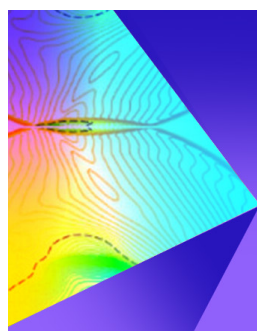
Physics of Fluids **34**, 031701 (2022); <https://doi.org/10.1063/5.0084646>

[Wall-bounded turbulent flows at high Reynolds numbers: Recent advances and key issues](#)

Physics of Fluids **22**, 065103 (2010); <https://doi.org/10.1063/1.3453711>

[A scaling improved inner-outer decomposition of near-wall turbulent motions](#)

Physics of Fluids **33**, 045120 (2021); <https://doi.org/10.1063/5.0046502>



Physics of Fluids

Special Topic: Shock Waves

Submit Today!

Reynolds number dependence of inner peak turbulence intensity in pipe flow

Cite as: Phys. Fluids **34**, 045103 (2022); doi: [10.1063/5.0084863](https://doi.org/10.1063/5.0084863)

Submitted: 10 January 2022 · Accepted: 10 March 2022 ·

Published Online: 4 April 2022






View Online



Export Citation



CrossMark

Marie Ono (小野 満里絵),^{1,2,a)}  Noriyuki Furuichi (古市 紀之),¹  Yuki Wada (和田 裕貴),³ Noboru Kurihara (栗原 昇),¹  and Yoshiyuki Tsuji (辻 義之)²

AFFILIATIONS

¹National Institute of Advanced Industrial Science and Technology, National Metrology Institute of Japan (AIST, NMIJ), Tsukuba 305-8563, Japan

²Department of Energy Engineering and Science, Nagoya University, Nagoya 464-8603, Japan

³Japan Atomic Energy Agency (JAEA), 2-4 Sirakata, Tokai-mura, Naka-gun, Ibaraki 319-1195, Japan

^{a)} Author to whom correspondence should be addressed: ono.marie@aist.go.jp

ABSTRACT

Streamwise turbulence statistics in the range from $Re_\tau = 990$ to $Re_\tau = 20750$ at the High Reynolds Number Actual Flow Facility at the National Metrology Institute of Japan are presented, specifically focusing on the Reynolds number dependence of the inner peak turbulence intensity. Velocity measurements are conducted using laser Doppler velocimetry (LDV), taking account of problems specific to this method, with the aim of providing reliable experimental results. The control volume and the fringe pattern of LDV, both of which influence turbulence statistics, are directly measured using a rotary wire device, and they are used to correct the measured turbulence intensity using methods developed in this study. The present results for mean velocity and turbulence intensity profiles agree well with direct numerical simulation data. The inner peak turbulence intensity in this pipe experiment increases with the increasing Reynolds number. It is found that the Reynolds number dependence of the inner peak up to $Re_\tau = 20750$ is very similar to that in a turbulent boundary layer (TBL). The slope of the outer logarithmic region in the turbulence intensity profile is twice the slope obtained from the relation between the inner peak and the Reynolds number. This relation is also consistent with that for TBL flow.

Published under an exclusive license by AIP Publishing. <https://doi.org/10.1063/5.0084863>

I. INTRODUCTION

Near-wall turbulence in wall-bounded flows has been studied for a long time from many aspects, including, for example, turbulence production and frictional drag. Among these, the local maximum value of the streamwise turbulence intensity, namely, an inner peak at $y^+ = yu_\tau/\nu \approx 15$, has attracted much interest.^{1–7} Here, y is the wall-normal position, u_τ is the friction velocity, and ν is the kinetic viscosity. According to the classical consideration, near-wall turbulence statistics is scaled by the inner variable, because the near-wall turbulent flow is dominated only by small-scale structures and is independent of the large structures in the outer layer. It is well known that the mean velocity profile in the near-wall region is well scaled by the inner variable. On the other hand, the inner peak value scaled by the inner variable increases with the increasing Reynolds number. For instance, DeGraaff and Eaton¹ reported a Reynolds number dependence of the peak value for turbulent boundary layer (TBL) flow. Since they assumed that large-scale structures in the outer region affected the inner peak turbulence intensity, they proposed a mixed scaling using

the friction velocity and the friction factor. Other recent papers have also reported that the peak values exhibit a notable dependence on the Reynolds number.^{8–10} Those results show a discrepancy with the classical wall scaling and indicate that the inner variable is not sufficient to scale the inner peak turbulence intensity.

To explain the growth of the inner peak, several scalings have been proposed. Lee and Moser³ and Marusic *et al.*⁴ suggested an interaction between the Reynolds number dependence of the inner peak and the outer region. They showed that the inner peak turbulence intensity increases logarithmically with the Reynolds number in channel and turbulent boundary layer (TBL) flows as follows:

$$(u^+)^2_{\max} = A_1 \ln Re_\tau + B. \quad (1)$$

Marusic *et al.* also noted the following logarithmic relation for the turbulence intensity in the outer region at a fixed Re_τ :

$$(u^+)^2 = A_2 \ln(y/R) + C, \quad (2)$$

where R is the outer scaling (the radius of the pipe in the case of pipe flow). This equation is based on the attached eddy model at high Reynolds number¹¹ and represents the profile in the outer region at $y/R \approx 0.1$. The smallest eddy size according to the attached eddy hypothesis coincides with the start point of the logarithmic region, which is $y^+ \propto Re_\tau^{0.5}$. Marusic *et al.* indicated that an increase in the smallest eddy size results in an increase in the inner peak. If the total streamwise turbulence intensity is assumed to be superposed on the viscous-scaled universal inner peak without any leakage of energy, then the relation $A_1 = A_2/2$ can be established. Marusic *et al.* reported values of $A_1 = 0.63$ and $A_2 = 1.26$ based on their experimental data for TBL flow (and then $B = 3.80$ and $C = 2.10$). On the other hand, Chen and Sreenivasan⁵ predicted that the growth of the peak value is finite, because the streamwise dissipation rate at the wall is finite. They considered the limit of the dissipation rate at the wall to be $\varepsilon^+ = 0.25$ ($\varepsilon^+ = \varepsilon\nu/u_\tau^4$). However, the energy dissipation rate is smaller than this limit at any finite Reynolds number. The proposed relation for the inner peak is

$$(u^+)_{\max}^2 = \alpha \left(\frac{1}{4} - \frac{\beta}{Re_\tau^{0.25}} \right), \quad (3)$$

where the constants were determined from direct numerical simulation (DNS) data of channel flow as $\alpha = 46$ and $\beta = 0.42$. Chen and Sreenivasan suggested that Eq. (3) also scales the inner peak in TBL and pipe flows. Both Eqs. (1) and (3) have been evaluated using many experimental and numerical data, but they have not been compared with each other directly at high Reynolds number. It is necessary to confirm which relation is appropriate. The values of the inner peak given by the two equations are close to each other until a certain Reynolds number, after which a difference appears at high Reynolds number. For example, the inner peak turbulence intensity calculated by Eq. (1) is only 0.4% different from that given by Eq. (3) at $Re_\tau = 10\,000$, but there is a 1.7% difference at $Re_\tau = 20\,000$. Thus, the difference increases with the increasing Reynolds number. To know which equation predicts the inner peak more precisely, accurately measured high Reynolds number experimental data are necessary. However, the values of the inner peak obtained in previous studies^{8–10,12} are more scattered at high Reynolds number than at low Reynolds number.

The most important and sensitive issue for the measurement of the turbulence intensity at high Reynolds number is the spatial resolution of the measurement device.¹³ The higher the Reynolds number, the higher is the required spatial resolution. The finite length of sensors in measurement devices imposes limitations on spatial resolution. This affects especially the turbulence intensity in the near-wall region. Hultmark *et al.*¹⁴ measured the streamwise turbulence intensity at $Re_\tau = 98\,190$ using a nanoscale thermal anemometry probe (NSTAP) in pipe flow. Although the spatial resolution was relatively high, they applied the correction procedure proposed by Smits *et al.*¹⁵ to the results in the near-wall region. The results that they found for the inner peak indicated that it was a constant, independent of Reynolds number, and thus were inconsistent with both Eqs. (1) and (3). Willert *et al.*⁹ presented turbulence intensity profiles in the near-wall region in pipe flow up to $Re_\tau = 39\,935$, obtained by particle image velocimetry (PIV). According to their results, the values of the inner peak increase with Reynolds number but gradually deviate from both Eqs. (1) and (3). Chen and Sreenivasan⁵ noted that these disagreements at high

Reynolds number were caused by insufficient spatial resolution of the measurement devices, but they did not give any criteria for the spatial resolution required to give a precise inner peak.

Another possible scenario for the disagreement in the behavior of the inner peak at high Reynolds number attributes this to differences in the geometry of the experimental facilities. Both Eqs. (1) and (3) provide good representations of experimental results for the inner peak in canonical flows (pipe, channel, and TBL) at low Reynolds number and in TBL flows at high Reynolds number. However, the values of the inner peak do not show consistency between different data in pipe flow at high Reynolds number. Hultmark *et al.*¹⁶ suggested that the discrepancy was caused by differences in the interaction between the inner and outer layers. However, the detailed mechanism of the interaction between the outer flow and the inner peak is still unclear. Moreover, there has not been a clear discussion of the inner peaks in TBL and pipe flows, because reliable experimental results are still insufficient.

The experiments described in this paper were conducted at the High Reynolds Number Actual Flow Facility (Hi-Reff) at the National Metrology Institute of Japan (NMIJ). Laser Doppler velocimetry (LDV) was chosen as the measurement device because the working fluid of this facility is water and LDV is a noninvasive measurement method with high spatial resolution. With careful consideration of the LDV-specific issues that affect turbulence statistics, we provide reliable experimental results for pipe flow up to $Re_\tau = 20\,750$. For this purpose, each aspect of the LDV system that affects turbulence statistics was evaluated based on actual measurements using a rotary wire device, and the turbulence intensity was estimated precisely using a correction method developed in this study.

We discuss the turbulence intensity profiles in pipe flow, focusing on two main aspects. The first of these is a check of the reliability of the turbulence intensity profile at low Reynolds number. Since the influence of issues connected with LDV increases with the increasing Reynolds number, measurements of turbulence statistics were carried out from low Reynolds number to confirm the reliability of the experimental results. In particular, DNS data at low Reynolds number are taken as a reference to confirm our measurements and processing procedures. Based on those reliability checks at low Reynolds number, the measurements were extended to higher Reynolds number. The second aspect is investigation of the Reynolds number dependence of the inner peak. The experimental results are compared with those of previous experiments and the empirical formulas in Eqs. (1) and (3) at high Reynolds number.

II. EXPERIMENTS

A. Experimental facility

The experiments were conducted using Hi-Reff at NMIJ. The details of this facility have been reported in previous studies.^{17,18} The working fluid is water at ambient temperature. The water temperature variation within a measurement of a single profile was less than $\pm 0.3\%$, and the effects of viscosity and density variation were negligibly small. In the present experiments, mean velocity and turbulence intensity profiles were measured through a borosilicate glass pipe of diameter 100 mm and streamwise length 250 mm in the window chamber. The step between the glass pipe and the upstream pipe was less than 0.1 mm. Upstream of the test section was a 90D length polished straight pipe. The roughness of this pipe was $Ra = 0.10\ \mu\text{m}$

($Ra^+ = u_\tau Ra/\nu = 0.04$), $Rz = 0.8 \mu\text{m}$ ($Rz^+ = u_\tau Rz/\nu = 0.3$). Further upstream, a 23D normal straight pipe with $Ra = 6.2 \mu\text{m}$ ($Ra^+ = 2.5$) and $Rz = 25 \mu\text{m}$ ($Rz^+ = 10$) was installed. In a previous study using the same facility, no influence of surface roughness was observed.¹⁷ The maximum friction Reynolds number was $Re_\tau = 20\,750$ and the maximum flow rate was $0.083 \text{ m}^3/\text{s}$. The friction velocity u_τ was calculated from the following equation:

$$u_\tau = \sqrt{\frac{\lambda}{8}} U_b, \tag{4}$$

where λ is the friction factor and U_b is the bulk velocity. In our previous study,¹⁷ we measured the friction factor λ at high Reynolds number based on the pressure drop and flow rate measurement and obtained the following equation:

$$\frac{1}{\sqrt{\lambda}} = 2.092 \log(Re_b \sqrt{\lambda}) - 1.176, \tag{5}$$

where $Re_b = U_b D/\nu$ is the bulk Reynolds number and D is the pipe diameter. The friction factor in the present paper is obtained using Eq. (5). The bulk velocity U_b was calculated from the flow rate and pipe diameter. A notable feature of this facility is its highly accurate measurement of flow rate using static gravimetric methods (the uncertainty is 0.04% with a coverage factor $k = 2$), and this contributes to the estimation of the friction factor, friction velocity, and Reynolds number. Another advantage of the facility is that stable flow can be achieved by a water supply from an overflow head tank of height 30 m. In this system, the risk of any artificial disturbance from the outside can be eliminated.

B. Measurement procedure

The streamwise velocity was measured by an LDV system. A solid-state laser with maximum power of 0.3 W and wavelength $\lambda = 532 \text{ nm}$ was used. The expanded uncertainty of the velocity measurement using this LDV system was estimated to be 0.2% with $k = 2$. The measurement positions in the glass pipe were calculated based on the refractive index, traverse position, and LDV parameters (focal length, beam spacing, and wavelength). The refractive index of the air

was 1.0003 and that of the glass pipe was 1.4751. The refractive index of water was corrected by the water temperatures during the measurements. The uncertainty of the wall position is estimated to be 5.4% ($k = 2$) at $y = 0.02 \text{ mm}$ and 1.2% ($k = 2$) at $y = 0.1 \text{ mm}$.

In general, streamwise velocities are measured aligned with the radial direction. However, measurement is impossible in the vicinity of the wall, because the laser beams are not able to reach there owing to the difference in the refractive indices. In this experiment, the line for the measurements was not aligned with the radial direction, but instead was slightly inclined to enable measurements in the near-wall region (as shown in Fig. 1). The velocities were measured at 48–58 positions along the measurement line. In the case of hot-wire (HW) measurements, the control length L (i.e., the length that directly affects the measured value) is taken as the spanwise length of the wire. In LDV measurements, the length of the control volume perpendicular to the wall affects the turbulence intensity. If the measurement line and the laser beam path intersect vertically, then the control length L that should be considered as representing the spatial resolution is just the minor diameter d of the control volume. However, when, as in Fig. 1, the laser beam path is not vertical to the measurement line, the major diameter l of the control volume also contributes to the control length L .

In these experiments, to investigate the influence of spatial resolution on LDV measurements, turbulence statistics were obtained at different spatial resolutions. The control length L was changed by two methods. One, shown in Fig. 1(a), involved changing the inclination angle θ of the measurement line. The streamwise velocities were measured for inclination angles of $\theta_1 = 15.1^\circ$ and $\theta_2 = 15.7^\circ$. With the increasing inclination angle θ , the control length L increases. The other method involved changing the focal length of the lens, as shown in Fig. 1(b). Measurements were taken with focal lengths of $f = 160 \text{ mm}$ and $f = 200 \text{ mm}$. With the increasing focal length, the control length L increases. The details of the measurement conditions are given in Table I. The Reynolds number differs slightly between cases #1, #2, and #3, but its deviation is within 3% (except for $Re_\tau = 2952$).

C. Rotary wire device

To evaluate the LDV parameters influencing turbulence statistics, a rotary wire device was used, as shown in Fig. 2(a). The details of the

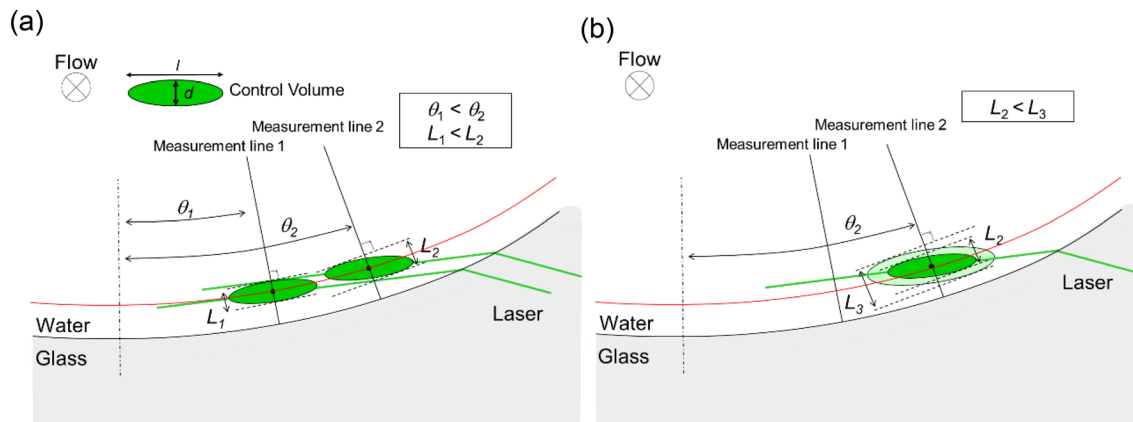


FIG. 1. Schematic of LDV measurements with different spatial resolutions. The control length L was changed by changing (a) the measurement line and (b) the focal length of the lens.

TABLE I. Measurement conditions. The difference in the measured Reynolds number of the three spatial resolutions is within 3% (except for $Re_\tau = 2952$). L and L^+ ($L^+ = Lu_\tau/\nu$) are the control lengths at $Re_\tau = 4270$ and $y^+ \approx 15$.

Case	Focal length f (mm)	Measurement line angle θ	L (μm)	L^+	Symbol in figures
#1	160	15.1°	60.1	5.04	Triangle
#2	160	15.7°	73.2	6.19	Square
#3	200	15.7°	100	8.66	Diamond

Reynolds number range $990 \leq Re_\tau < 20\,750$

device have been reported previously.^{19,20} It calibrates an LDV system using the rotational speed of a tungsten wire of diameter $5\ \mu\text{m}$. The rotational speed is determined by a pulse encoder and the distance between the center of the rotor and the wire. The rotor moves in $1\ \mu\text{m}$ intervals in the direction of the laser beam, i.e., the z axis direction. The burst signals when the wire passes the control volume of the LDV are analyzed by a digital oscilloscope and a signal processing device. The

center of the control volume is determined from the amplitude obtained from the digital oscilloscope at each position in the control volume.

This device is suitable for the velocity range from 1.3 to 40 m/s. The combined standard uncertainty of the calibration is estimated to be 0.01% ($k = 2$) in the velocity range from 2 to 30 m/s. The LDV system used in the present experiments was examined in the velocity range from 1.3 to 10 m/s (the maximum velocity was 12.3 m/s at $Re_\tau = 20\,750$). This device was used not only to measure the absolute velocity, but also to determine the major diameter l and the fringe distortion of the control volume, which will be explained in Sec. III. The velocity correction coefficient, the fringe distortion, and the control volume were determined for each lens ($f = 160\ \text{mm}$ and $f = 200\ \text{mm}$) individually.

The absolute velocity was corrected by a convergence coefficient C_f which was obtained from a comparison between the velocity indicated by the LDV system and the rotational speed to the wire. It was applied to values of both the mean velocity and the turbulence intensity in all measurement regions across the pipe. The coefficients for $f = 160$ and $f = 200$ were $C_f = 1.004\,45$ and $C_f = 0.996\,564$, respectively. All examined results were first corrected using the convergence coefficients.

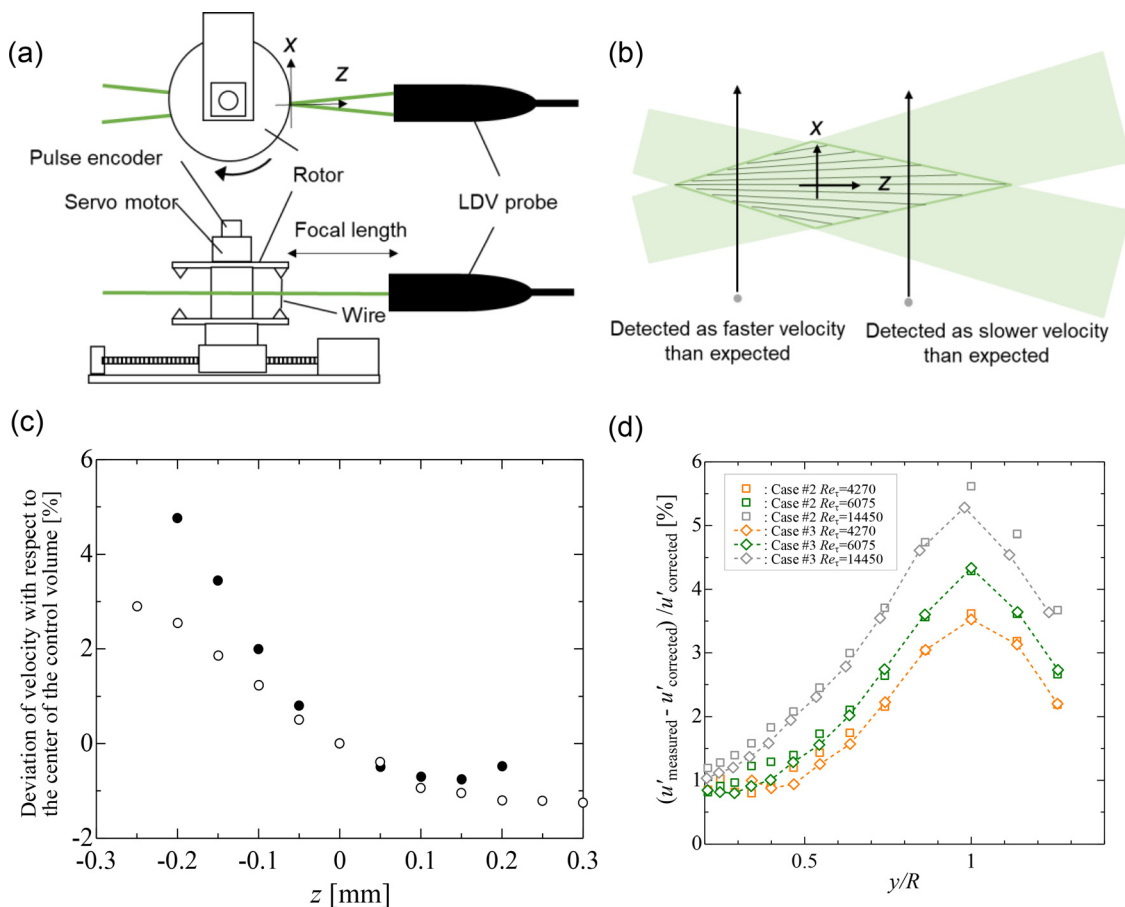


FIG. 2. (a) Schematic of rotary wire device. (b) Image of the fringe distortion in the control volume. (c) Fringe distortions for $f = 160$ (solid circles) and $f = 200$ (open circles) in this experiment as evaluated by the rotary wire device. (d) Measured deviation with respect to the corrected u' , considering fringe distortion in cases #2 and #3 at each wall-normal position. The orange, green, and gray plots are at $Re_\tau = 4270, 6075,$ and 14450 , respectively.

III. LDV MEASUREMENTS AT HIGH REYNOLDS NUMBER

A. LDV-specific issues

In this study, we measured the streamwise turbulence intensity profiles in pipe flows up to $Re_\tau = 20750$ by LDV to provide precise experimental results and investigate the Reynolds number dependence of the inner peak turbulence intensity. In previous studies at Hi-Reff, the mean velocity profiles were measured up to $Re_\tau = 53\,000$ by LDV, and it was found that the value of the Kármán constant asymptotically approached a constant value of $\kappa = 0.384$.^{17,21} In the present study, the turbulence intensity profiles were measured. To provide highly reliable results, several aspects of the LDV system that affect turbulence statistics were investigated based on actual measurements using the rotary wire device. HW and PIV measurements, which were used in previous high-Reynolds-number experiments, underestimate the turbulence intensity. Conversely, LDV overestimates the turbulence intensity because of the spatial resolution.

LDV has been applied to many flow fields, including wall-bounded flows, and is recognized as one of the tools that is applicable to near-wall turbulence measurements.^{22–24} However, previous studies have been limited to low Reynolds number experiments. Owing to the issue of spatial resolution, in previous studies, the Reynolds number of wall bounded flows has been $Re_\tau = 6000$ at most.^{22,25–27} It is necessary to take careful consideration of the factors influencing measurement devices. Usually, these factors are inherent to each method, such as hot-wire measurements, PIV, and LDV.

There are three factors in LDV measurements that affect turbulence statistics, and they can be summarized as follows:

1. Particle passing frequency: this leads to overestimation of the mean velocity and over- or underestimation of the turbulence intensity.
2. Spatial resolution: this leads to overestimation of the turbulence intensity because of the finite control volume together with the difficulty in determining its actual dimensions.
3. Fringe distortion: this leads to overestimation of the turbulence intensity because of the nonuniform fringe pattern inside the control volume.

With regard to the first issue, since LDV detects the velocities of particles passing through the control volume, the sampling frequency is not uniform. It is high around the pipe center but low near the wall, in general, since the number of particles that pass through the control volume increases with particle velocity. Consequently, the arithmetic mean velocity is positively biased from the true one. To avoid this effect, the mean velocity and turbulence intensity are generally corrected using a weighting factor g_i as follows:²⁸

$$U = \frac{\sum_{i=1}^n u_i g_i}{\sum_{i=1}^n g_i}, \tag{6}$$

$$u' = \sqrt{\frac{\sum_{i=1}^n (u_i - U)^2 g_i}{\sum_{i=1}^n g_i}}, \tag{7}$$

where u_i is the velocity of each particle and n is the number of samples. In this experiment, the transit time at which the particle passes the control volume is used as the weighting factor g_i in this correction.

As far as the second issue is concerned, in general, the turbulence intensity is affected by the spatial resolution. In the case of HW measurements, velocity fluctuations are averaged over the sensitive length l , and small-scale or high-frequency fluctuations are attenuated. Therefore, the measured turbulence intensity is underestimated. This is usually understood as the spatial resolution problem.^{13,15} Several correction methods have been proposed for HW measurements based on experimental data on the different spatial resolutions using the same facility, DNS data, and so forth.^{29–33} Conversely, in the case of LDV, the spatial resolution affects the turbulence intensity in a different way. Near the wall, where large velocity gradient exists, the turbulence intensity is overestimated. Durst *et al.*²² suggested the following correction for this effect:

$$U_{\text{meas}} = U_{cv} + \frac{L^2}{32} \left(\frac{d^2 U_{cv}}{dy^2} \right), \tag{8}$$

$$u_{\text{meas}}^2 = u_{cv}^2 + \frac{L^2}{16} \left(\frac{dU_{cv}}{dy} \right)^2 + \frac{L^2}{32} \left(\frac{d^2 u_{cv}^2}{dy^2} \right), \tag{9}$$

where U_{meas} and u_{meas}^2 are the measured mean velocity and turbulence intensity, U_{cv} and u_{cv}^2 are, respectively, the mean velocity and turbulence intensity at the center of the control volume, and L is the control length, which directly affects the measured value. The mean velocity and turbulence intensity at the center of the control volume are estimated from these relations using the measured data. However, these relations have only been applied to low Reynolds number, but not (as far as the present authors know) to high Reynolds number wall-bounded flows. Recently, another method to estimate the turbulence intensity at the center of the control volume has been reported. It is based on the probability density function (PDF) of the streamwise velocity at each position across the pipe.^{34,35} The principle of this method is completely different from that of Durst *et al.*²² However, in both methods, it is necessary to determine the control length L .²⁵ It is not easy to determine the actual control length L , because the beam intensity of LDV is not uniform, but has a Gaussian distribution inside of the control volume. A general method to calculate the control volume in the ideal case can be found in the previous study,²⁸ but it needs to be improved to take account of the actual measurement field. Especially at high Reynolds number with large velocity gradient, the influence of the control volume is significant. A small misestimate of the control length L will lead to an over- or underestimated turbulence intensity, even if Eq. (9) is used. In this paper, a new approach to obtain the control volume precisely using measurement results is proposed. The details will be given in Sec. III C.

Finally, in addition to the spatial resolution, it is necessary to consider the effect of the fringe distortion on LDV measurements. Fringe distortion is generated by manufacturing problems, such as deviations from beam parallelism and lens aberrations. Turbulence intensity is generally overestimated by the fringe distortion because different particle velocities are obtained from nonuniform fringe patterns. If the fringe pattern is distorted, the measured particle velocity changes according to the location in the control volume.³⁶ The spatial resolution caused by the velocity gradient affect mainly the inner region, but

the effects of fringe distortion are stronger in the outer region. These two effects occur independently in LDV measurements. The velocity gradient effect is larger than the fringe distortion effect near the wall, but the reverse is the case in the outer region. In this paper, a new method to evaluate the influence of fringe distortion is introduced in Sec. III B.

B. Evaluation of fringe distortion

The fringe pattern in the control volume of an LDV system is constructed by the crossing condition of two laser beams. In principle, if the laser beam diameter is uniform at any position, the fringe distance is not distorted in the control volume. However, the beam diameter is a function of the distance along the beam path, as shown in Fig. 2(b). This induces fringe distortion. When fringe distortion occurs, the turbulence intensity is overestimated, because particles that actually have the same velocity are detected as having different velocities depending on the position in the control volume through which they pass, as shown in Fig. 2(b). The influence of the fringe distortion has been investigated by Durst *et al.*³⁶ Since the fringe distortion varies from device to device, it needs to be determined individually for each measurement device.

In the present experiments, the fringe distortion was investigated using the rotary wire device. The fringe distortion was evaluated by traversing the position of the rotor with the wire. A comparison of the velocity measured by the LDV system and the actual rotational speed of the wire is shown in Fig. 2(c). There is a difference between these measurements, and this depends on the position inside the control volume. The maximum deviations from the center of the control volume are 4.8% and 2.9% at $f=160$ and $f=200$, respectively. The influence of the fringe distortion on the mean velocity is not great, because the velocities measured are averaged across the control volume in the z direction. However, the turbulence intensity will be affected. The fringe distortion effect occurs at any measurement position in the pipe, but it is smaller than the effect of the velocity gradient. Thus, the fringe distortion effect is significant except near the wall.

The fringe distortion effect is corrected using the PDF of the velocity fluctuation. We define the PDF $P_A(u; \mathbf{x})$ measured at $\mathbf{x} = (x, y, z)$ [for coordinates, see Figs. 2(a) and 2(b)], where u is the streamwise velocity. Subscript A indicates the area in the (y, z) plane. The actual PDF $P_M(u; V)$ measured by LDV is given by the integral of $P_A(u; \mathbf{x})$ over the control volume V :

$$P_M(u; V) = \frac{1}{V} \int_V P_A(u; \mathbf{x}) dV. \tag{10}$$

This approach was proposed by Wada *et al.*^{34,35} When the velocity field is homogeneous in the (x, y) plane, Eq. (10) reduces to

$$P_M(u; V) = \frac{1}{V} \int_{-l/2}^{l/2} P_A(u; z) s(z, V) dz, \tag{11}$$

where l is the major diameter of the control volume, and $s(z, V)$ is the area of the control volume at the z position. The base PDF P_B is defined as the PDF of the normalized velocity $[u - U(z)]/\sigma(z)$, where $U(z)$ is the mean velocity and $\sigma(z)$ is the standard deviation at z , and $P_A(u; z)$ is then expressed as

$$P_A(u; z) = \frac{P_B([u - U(z)]/\sigma(z))}{\sigma(z)}, \tag{12}$$

where $U(z)$ and $\sigma(z)$ are given by

$$U(z) = [1 + f(z)]U(0), \tag{13}$$

$$\sigma(z) = [1 + f(z)]\sigma(0), \tag{14}$$

in which $f(z)$ is determined by the actual measurement results as shown in Fig. 2(c). The PDF of the infinitesimal volume at the center of the control volume is determined to satisfy Eq. (11), and the standard deviation is calculated from that PDF. The basic procedure to obtain PDF is the same as that of our previous paper.³⁴

The influence of the fringe distortion based on Eq. (11) is shown in Fig. 2(d), where the results are those for case #2 measured by a lens with $f=160$ and for case #3 measured by a lens with $f=200$ at three Reynolds numbers. The correction effect for the two different focal lengths is almost the same at $Re_\tau = 4270$ and 6075 . However, case #2 with $f=160$ has a slightly larger correction around the center at $Re_\tau = 14450$ than case #3 with $f=200$. This is because the lens with $f=160$ has a greater fringe distortion than that with $f=200$, as shown in Fig. 2(c). The influence of the fringe distortion is significant in the outer region of the boundary layer, as shown in Fig. 2(d). It should be noted that this proposed estimation (or correction) procedure for the actual turbulence intensity is important for confirming the relation between the slope of the logarithmic region in the outer layer as expressed by Eq. (2) and the slope of the Reynolds number dependence of the inner peak in Eq. (1). The slope A_2 in Eq. (2) is clearly influenced by fringe distortion.

C. Determination of control length L

Since the turbulence intensity is overestimated by a finite control volume, it is necessary to establish a correction procedure to estimate the expected values. As mentioned in Sec. I, the control length L is key parameter in those procedures.^{25,26} Precise determination of the control length L is very important for an accurate estimation and for providing a reliable turbulence intensity. A method for determining the control length L has been found in previous studies.^{25,26} It uses the relation between the mean velocity gradient and the turbulence level measured in a laminar flow. However, this method has a limitation due to the dynamic range of the measurement device and the fringe distortion mentioned above. For high Reynolds number measurements, the required measurement range of the velocity is large. Since the uncertainty of velocity measurement increases with decreasing velocity, this method is not suitable for precise determination of the control volume. Therefore, we determined the control length L by using the rotary wire device.

Figure 3(a) shows the distribution of the amplitude of the burst signal as the wire passes through each position in the measurement volume. This distribution can be regarded as that of the laser beam power inside the control volume. In general, the waist diameter of the laser beam is defined as being at the position where its power is e^{-2} of the maximum. According to this definition, the major diameter l of the control volume is tentatively obtained from the e^{-2} point of the amplitude distribution, as shown in Fig. 3(a). However, as shown in Fig. 3(c), the corrected turbulence intensities based on the control length L determined by the e^{-2} point slightly differ between the three

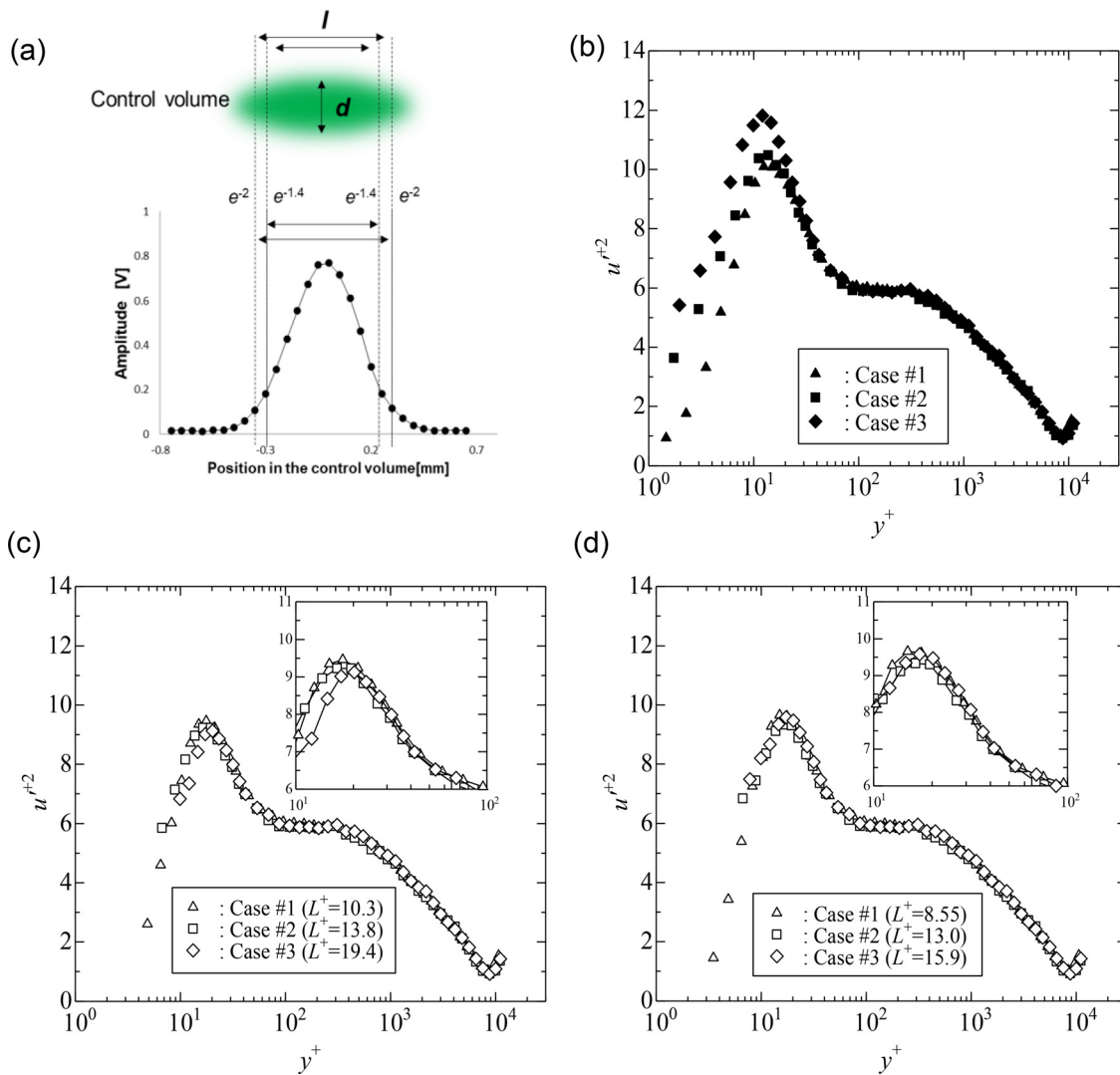


FIG. 3. (a) The major diameter l of the control volume is determined by the distribution of amplitude as the wire passes through each position. (b) Turbulence intensity profiles without correction for the spatial resolution at $Re_\tau = 8610$. Note that the data have already been corrected for the weighting factor and the fringe distortion. (c) and (d) Corrected results based on the estimation according to Eq. (9) using control lengths L determined by the $e^{-1.4}$ and e^{-2} points, respectively.

cases [Fig. 3(b) shows turbulence intensity profiles without correction for the spatial resolution]. On the other hand, the turbulence intensities obtained from a control length L determined by the $e^{-1.4}$ point agree well between the three cases, as shown in Fig. 3(d). The reason why the $e^{-1.4}$ threshold works better may be connected with a difference in measurement conditions. Since the laser beam passes through water and a glass pipe, the beam power will be attenuated under the actual measuring conditions. Taking this into account, the major diameter l of the control volume can be determined by the $e^{-1.4}$ point. Once the major diameter l of the control volume has been determined, the minor diameter d is obtained as follows:

$$d = \frac{l \sin \phi}{\cos \phi}, \tag{15}$$

where ϕ is the half-intersection angle of the beams. The control length L is calculated geometrically from the major diameter l , the minor diameter d , and the inclination angle of the control volume with respect to the measurement line (see Fig. 1). The measurement conditions are summarized in Table I.

A comparison between raw (uncorrected) and corrected turbulence intensities for different spatial resolutions is shown in Fig. 4. Durst *et al.*²² limited their considerations to data obtained when more than half of the control volume was inside the working fluid, owing to the increased electric and optical noise. We adopt the same procedure, and the corrected turbulence intensity in the near-wall region is not shown in the figure. At $Re_\tau = 2084$, the effect of the spatial resolution is confirmed only in the viscous sublayer in case #3 ($L^+ = 4.92$) with the largest control length L [Fig. 4(a)]. At $Re_\tau = 6075$, this effect

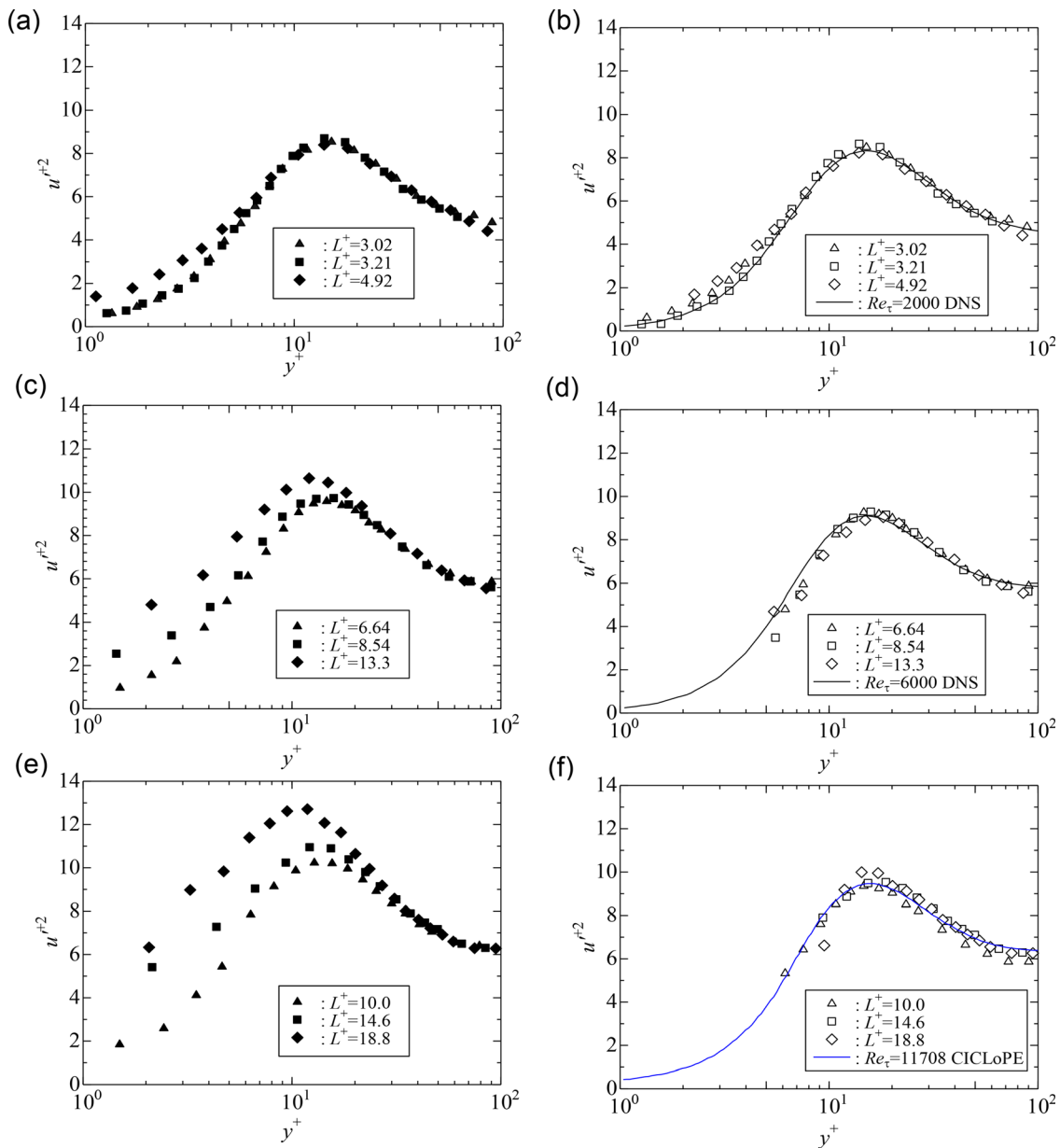


FIG. 4. Turbulence intensity profiles in the inner region for three different spatial resolutions. (a) and (b) Raw (uncorrected) and corrected results based on Eq. (9) at $Re_\tau = 2084$. The black solid line in (b) shows the pipe flow DNS data from Chin *et al.*³⁷ (c) and (d) Results at $Re_\tau = 6075$. The black solid line in (c) shows the pipe flow DNS data from Pirozzoli *et al.*³⁸ (e) and (f) Results at $Re_\tau = 11\ 040$. The blue solid line in (f) shows the pipe flow experimental results from CICLoPE.⁹

appears clearly not only in the viscous sublayer but also around the inner peak, at $y^+ \approx 15$ [Fig. 4(c)]. However, the turbulence intensity profiles measured at the three different spatial resolutions are in good agreement with one another by correction. Moreover, they are also in good agreement with DNS data from Chin *et al.*³⁷ and Pirozzoli *et al.*³⁸ [Figs. 4(b) and 4(d)]. The spatial resolution has a remarkable effect on the turbulence intensity at $Re_\tau = 11\ 040$ [Fig. 4(e)]. However, the corrected results for the three different spatial resolutions are good

agreement with each other and are similar to results from the CICLoPE facility at the University of Bologna, Italy⁹ [Fig. 4(f)].

IV. EXPERIMENTAL RESULTS AND DISCUSSION

In this section, the turbulence statistics measured with LDV-specific effects taken into account are presented. The discussion focuses mainly on the mean velocity and the turbulence intensity

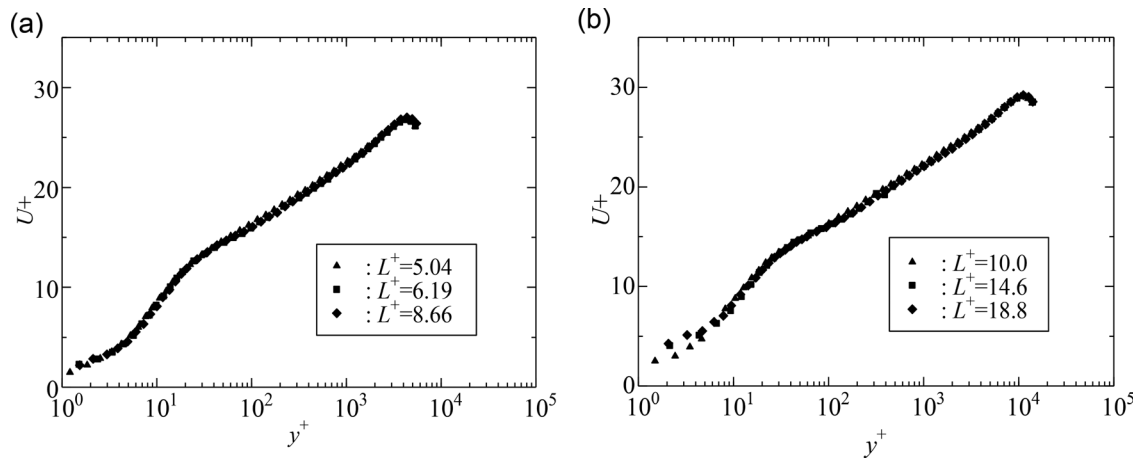


FIG. 5. Mean velocity profiles for three different spatial resolutions at (a) $Re_\tau = 4270$ and (b) $Re_\tau = 11040$.

profiles of the streamwise component from $Re_\tau = 990$ to $Re_\tau = 20750$. The Reynolds number dependence of the inner peak is also discussed.

A. Mean velocity

Mean velocity is affected by the spatial resolution only in the viscous sublayer. To investigate the influence of the spatial resolution, the mean velocity profiles measured at $Re_\tau = 4270$ and $Re_\tau = 11040$ for three different spatial resolutions are shown in Fig. 5. The data shown in the figure are corrected only by the weighting factor. The influence of the spatial resolution does not appear at $Re_\tau = 4270$, but a small influence emerges in the viscous sublayer at $Re_\tau = 11040$. Except in the near-wall region, the influence of the spatial resolution is not confirmed.

The mean velocity profiles in the range from $Re_\tau = 990$ to $Re_\tau = 20750$ are shown in Fig. 6. The results from the wall to the buffer layer in case #1 are combined with data from the buffer layer to the center of case #3 as the complete dataset for the turbulence statistics, because the inner region is susceptible to the influence of the spatial resolution and the outer region to that of the fringe distortion. In this result, the LDV-specific effects, namely, the passing frequency of the particles, the spatial resolution, and the fringe distortion, are corrected as described in Sec. III. The measured profiles overlap sufficiently at $y^+ > 100$. Using the indicator function $\Xi = (y^+ du^+ / dy^+)^{-1}$, the Kármán constant is calculated from the velocity profile, where Ξ is a constant that is equal to 0.380 for $Re_\tau = 20750$. This value is slightly smaller than a previous result of 0.382 at $Re_\tau = 20000$.¹⁷ However, they agree with each other within the experimental uncertainty. The experimental results are also good agreement with DNS data on channel flow from Yamamoto and Tsuji³⁹ rather than with data on pipe flow from Pirozzoli *et al.*³⁸

B. Turbulence intensity profile

The turbulence intensity profiles are shown in Fig. 7, together with the results from previous studies. The present results are in good agreement with pipe flow DNS data from Chin *et al.*³⁷ and Ahn *et al.*⁴⁰ at $Re_\tau = 990, 2084, \text{ and } 2952$, and also agree with DNS data

from Pirozzoli *et al.*³⁸ at $Re_\tau = 6075$, although a small difference is observed from $y^+ = 100$ to 400. At higher Reynolds number, the present results agree well with channel flow DNS results from Yamamoto and Tsuji.³⁹ The difference observed in the outer region is due to the small difference in Reynolds number between experiment ($Re_\tau = 8610$) and DNS ($Re_\tau = 8000$), and due to the difference of geometries. Thus, the comparison between the present data and DNS profiles shows consistency from $Re_\tau = 990$ to $Re_\tau = 8610$.

Willert *et al.*⁹ reported that the outer peak appears at $y^+ = 200\text{--}400$ for $Re_\tau \leq 20000$. The turbulence intensity grows in this region depending on the Reynolds number, but a clear outer peak is not observed in the present results.

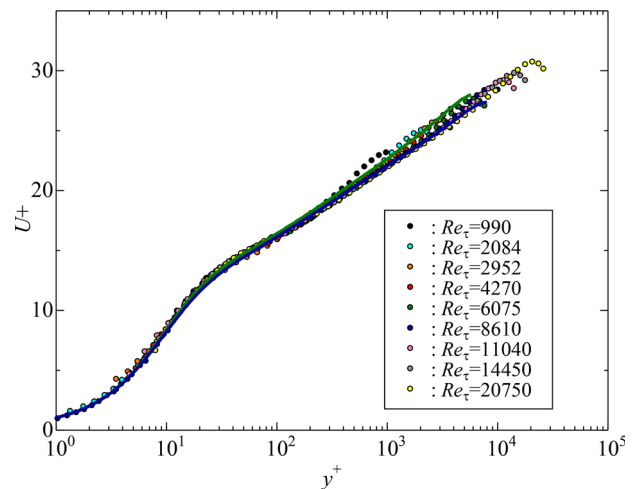


FIG. 6. Mean velocity profiles at $Re_\tau = 990$ to $Re_\tau = 20750$, combining the results for cases #1 and #3 around the buffer region. The green solid line shows pipe flow DNS data from Pirozzoli *et al.*³⁸ and the blue solid line shows channel flow DNS data from Yamamoto and Tsuji.³⁹

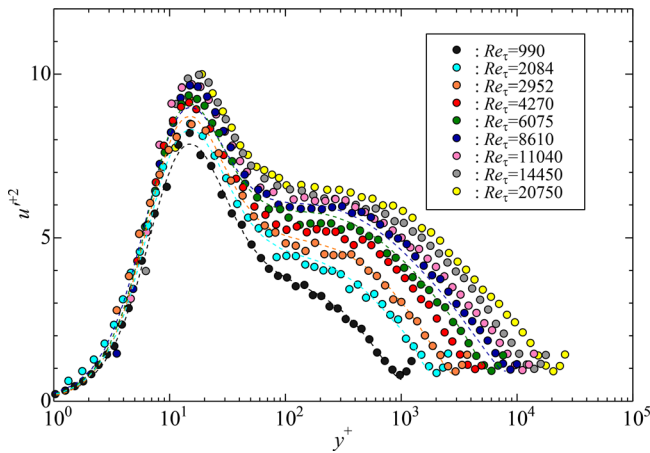


FIG. 7. Turbulence intensity profiles at $Re_\tau = 990$ to $20\,750$, combining the results of cases #1 and #3. The effects of the spatial resolution and the fringe distortion are corrected. The dashed lines show DNS data from Chin *et al.*³⁷ at $Re_\tau = 1002$ and $Re_\tau = 2003$, Ahn *et al.*⁴⁰ at $Re_\tau = 3008$, Pirozzoli *et al.*³⁸ at $Re_\tau = 6000$, and Yamamoto and Tsuji³⁹ at $Re_\tau = 8000$.

C. Reynolds number dependence of the inner peak turbulence intensity

Figure 8(a) shows the inner peak turbulence intensity of three different spatial resolutions vs the Reynolds number. The effects of the spatial resolution are observed clearly from $Re_\tau = 4200$ and increase with increasing Reynolds number. However, the corrected values for the different spatial resolutions coincide with one another up to $Re_\tau = 14\,000$. The corrected values of the inner peak for the three cases are within $\pm 2.4\%$ from $Re_\tau = 2000$ to $Re_\tau = 14\,000$, but this range is $\pm 5.5\%$ at $Re_\tau = 20\,000$.

Two scaling formulas for the Reynolds number dependence of the inner peak were mentioned in Sec. I, namely, the logarithmic

relation of Eq. (1) and the asymptotic relation of Eq. (3). Both equations are fitted to the present data up to $Re_\tau = 14\,000$ and the coefficients determined as follows:

$$(u'^+)_{\max}^2 = 0.72 \ln Re_\tau + 3.01, \tag{16}$$

$$(u'^+)_{\max}^2 = 46 \left(\frac{1}{4} - \frac{0.44}{Re_\tau^{0.25}} \right). \tag{17}$$

These equations are plotted as the dotted and dashed lines, respectively, in Fig. 8(a).

Since the corrected values of the inner peak are scattered at high Reynolds number, it seems that there is a correctable or measurable limitation on the control lengths L^+ in this experiment. The deviation of the corrected results from Eq. (17) is plotted against the control length L^+ in Fig. 8(b). The deviation from Eq. (17) is less than $\pm 5\%$ for $L^+ \leq 25.0$, but it exceeds $\pm 5\%$ for $L^+ \geq 25.8$. Similarly, when the deviation from Eq. (16) is calculated, the results exceed $\pm 5\%$ for $L^+ \geq 25.8$. This indicates that the values measured for $L^+ \geq 25.8$ in this experiment deviate greatly from the expected value. To distinguish the results at large spatial resolution, those for $L^+ \geq 25.8$ in Fig. 8(a) are shown by half-filled gray symbols. For HW measurements, the limit of correction has been reported as $L^+ < 20$.¹³ Although this limit is slightly smaller than that for LDV, it is interesting that they have similar values.

For HW measurements, inner peak turbulence intensities measured at the same facility and corrected by different methods were compared by Miller *et al.*⁴¹ It is important to compare the results of different correction methods to evaluate the validity of these corrections. In our previous study,³⁴ another correction method was proposed based on the PDF of the velocity fluctuation (this is hereinafter referred to as Wada’s method). In that study, Wada’s method was applied up to $Re_\tau = 10\,400$, with the control volume calculated by the LDV parameters. Here, we update these previous results using the precise size of the control volume obtained in this paper and applied up to $Re_\tau = 20\,750$. A comparison between the present results and those

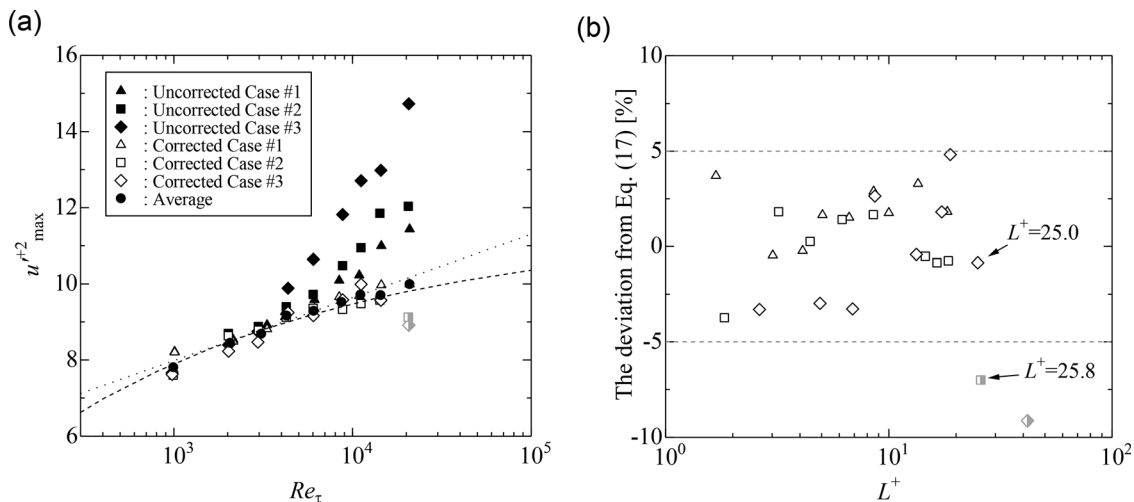


FIG. 8. (a) Reynolds number dependence of the inner peak turbulence intensity. The black filled circles represent the average of the corrected results in the three cases for $L^+ < 25.0$ (excluding the results indicated by half-filled gray symbols). The dotted line is Eq. (16) and the dashed line is Eq. (17). (b) Deviation of the corrected results from Eq. (17) for each L^+ . Half-filled gray symbols are the results $> 5\%$.

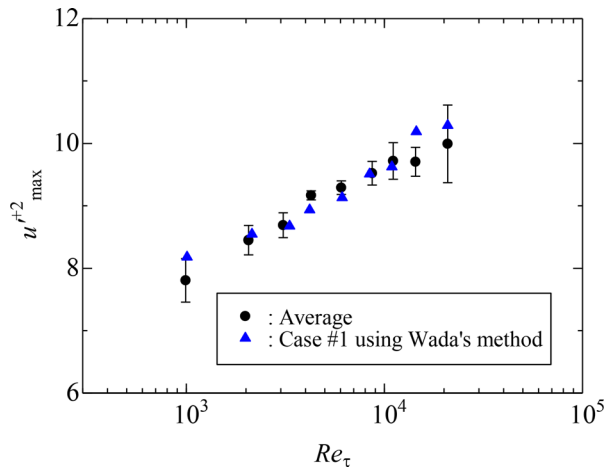


FIG. 9. Inner peak turbulence intensities corrected for case #1 using Wada's method. The black filled circles are the same as those in Fig. 8(a).

using Wada's method is shown in Fig. 9. While some results do not overlap within the uncertainty level, most of the results corrected by the two different methods agree acceptably with each other in the examined Reynolds number range.

The inner peak values are compared with previous DNS^{1,8–10,14,38–40,42} and experimental data in Fig. 10. The present results measured by LDV do not show any plateau and increase depending on the Reynolds number. This tendency is different from that found in previous experiments on pipe flow, which deviated from Eqs. (1) and (3) at high Reynolds number.^{9,14} On the contrary, the present results are closer to the profile of TBL flows. In particular, they are consistent with the results for a TBL obtained by Samie *et al.*¹⁰ using a fully resolved NSTAP with $L^+ = 2.4–3.5$. It is remarkable that Samie *et al.* did not apply correction to their HW measurements. The consistency between the two sets of experimental results is worthy to give a reliable inner peak for the near-wall turbulence, since this consistency indicates that the inner peak is independent of the geometry for canonical flows at least up to $Re_\tau = 20\,000$. Focusing on the pipe flow, the present results are similar to those from CICLoPE at low

Reynolds number, but the trends in the higher Reynolds number region seem to be different.

The present results are intermediate between those given by Eqs. (1) and (3), respectively. Although these empirical equations represent the present results well, including those at low Reynolds number, it is difficult to decide which equation predicts the inner peak precisely. The higher Reynolds number results are needed to determine which scaling expresses the Reynolds number dependence more accurately. In this study, the slope of Eq. (1) is $A_1 = 0.72$, as shown in Eq. (16). This result is very close to that of the previous study by Marusic *et al.*,⁸ which gave $A_1 = 0.7$. Note that this value was slightly changed to $A_1 = 0.63$ in a later publication by the same authors.⁴ The constants in Eq. (3) were obtained as $\alpha = 46$ and $\beta = 0.44$, as in Eq. (17). α is related to a finite value of the inner peak when $Re \rightarrow \infty$, as reported by Chen and Sreenivasan.⁵ According to their assumption, the maximum value of the inner peak is predicted as $u_{max} = \alpha/4 = 11.5$ from the value of $\alpha = 46$. On the other hand, β is slightly different from that obtained by Chen and Sreenivasan, and they also suggested that β may depend on the geometry. In the present experiments, the value of β was slightly larger than that previously obtained from DNS of channel flow.

D. Logarithmic region in outer layer

According to the attached eddy model, the turbulence intensity profile at high Reynolds number has a logarithmic region given by Eq. (2). Marusic *et al.*⁴ indicated that the slope A_1 , which is associated with the Reynolds number dependence of the inner peak, is half of the slope A_2 of the logarithmic region in the outer region of TBL. The turbulence intensity profiles with respect to the outer variables are shown in Fig. 11. The logarithmic region can be clearly observed around $y/R = 0.1$, especially at high Reynolds number. Assuming the slope A_2 of the logarithmic region to be twice the value $A_1 = 0.72$ from Eq. (16) gives $A_2 = 1.44$. From the fit taking $A_2 = 1.44$, the equation based on the attached eddy model gives the relation $(u^+)^2 = 1.70 - 1.44 \ln(y/R)$. This equation expresses correctly the results in the logarithmic region as given by the solid line in Fig. 11. Thus, it is found that the relationship between the Reynolds number dependence of the inner peak and the logarithmic region with $A_1 = A_2/2$ is also satisfied in pipe flow, although the values of the constants A_1 and A_2 are different from those in a TBL.

Finally, we emphasize that the relationship between the inner peak and the logarithmic region in the present data is confirmed by a

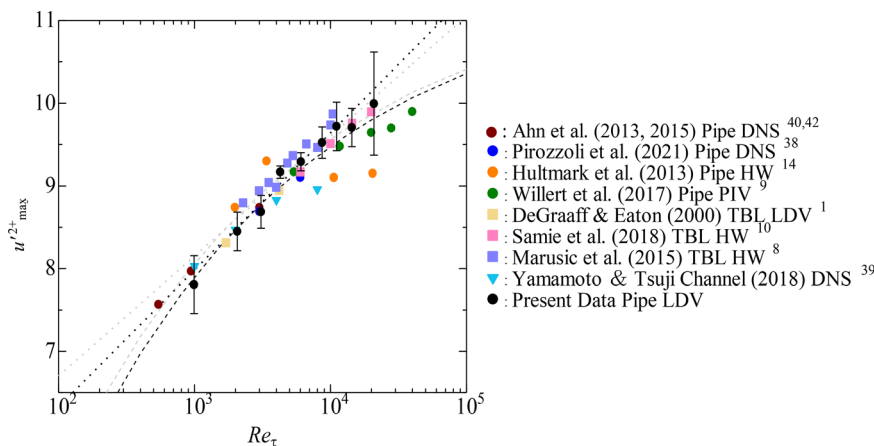


FIG. 10. Comparison of the Reynolds dependence of the inner peak turbulence intensity with the results of previous studies. The black dotted line is Eq. (16), and the black dashed line is Eq. (17). The gray dotted line is $(u^+)_{max}^2 = 0.63 \ln Re_\tau + 3.80$ according to Marusic *et al.*⁴ The gray dashed line is $(u^+)_{max}^2 = 46(1/4 - 0.42/Re_\tau^{0.25})$ according to Chen and Sreenivasan.⁵ The error bars indicate the uncertainty calculated by the variation among three different spatial resolutions.

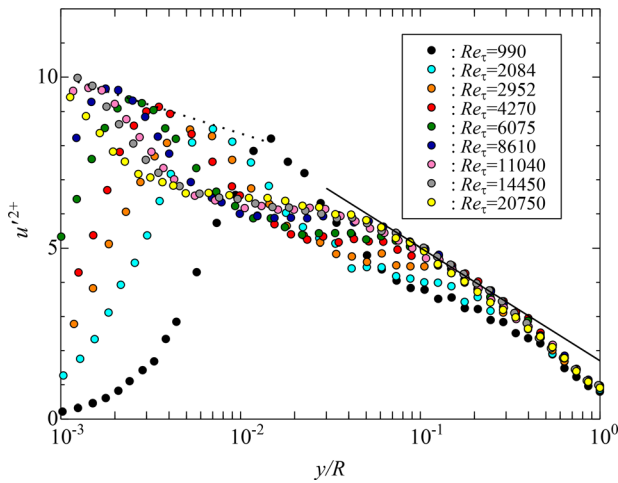


FIG. 11. Turbulence intensity profiles for outer scaling. The dotted line is $(u'^2+)_{\max} = 5.04 - 0.72 \ln(y/R)$ and the solid line is $(u'^2+) = 1.70 - 1.44 \ln(y/R)$.

careful consideration of the correction of LDV-specific problems, such as the spatial resolution and the fringe distortion. Örlü *et al.*⁴³ mentioned the relation $A_1 = A_2/2$ for the HW measurement results at CICLoPE, but this was not based on a strict analysis of the turbulence intensity profile. In the present study, careful measurements and the application of corrections based on an actual evaluation using the rotary wire device have led to reliable experimental results.

V. CONCLUSIONS

LDV measurements of turbulence statistics for the streamwise component in pipe flow from $Re_\tau = 990$ to $Re_\tau = 20750$ have been conducted, with careful account taken of specific issues associated with this method, particularly spatial resolution. To improve the correction and measurement results, a rotary wire device has been used to examine these specific issues influencing turbulence statistics. The factors taken into consideration are the velocity correction coefficient C_f , which affects the absolute value of velocity, the fringe distortion, and the control length L . A new correction procedure considering the LDV fringe distortion has been proposed. The corrected turbulence intensity profiles based on each parameter agree acceptably well with DNS data. The turbulence intensities of the inner peak measured for three different spatial resolutions are consistent with each other (within $\pm 2.4\%$ from $Re_\tau = 2084$ to 14450). The measurement accuracy decreases when control lengths $L^+ \geq 25.8$ are used.

The present experimental results indicate that the inner peak turbulence intensity increases with increasing the Reynolds number. They agree well with experimental results for a TBL reported by Samie *et al.*¹⁰ up to $Re_\tau = 20000$, rather than with previous results for pipe flow. The previous pipe flow data deviate from the logarithmic relation given by Eq. (1) and the asymptotic relation given by Eq. (3) at high Reynolds number. The consistency between the pipe flow and TBL results is worthy to give a reliable peak value for near-wall turbulence, because it indicates that the peak value is independent of the geometry of the canonical flow.

Regarding the relation between the inner peak and the logarithmic region of the turbulence intensity profiles, the slope of the inner

peak is found to be a half of the slope of the turbulence intensity profile in the outer region. This relation is the same as that for TBL. Finally, we should emphasize that these results are based on a careful consideration of LDV-specific problems, such as the spatial resolution and the fringe distortion.

ACKNOWLEDGMENTS

The authors are grateful to Dr. M. Juling and Mr. F. Heitmann at Physikalisch-Technische Bundesanstalt for their helpful discussions of the LDV issues. This research was partially supported by the Ministry of Education, Science, Sports, and Culture, Grant-in Aid for Scientific Research, Fostering Joint International Research (B), 2019–2022 (No. 19KK0098).

AUTHOR DECLARATIONS

Conflict of Interest

The authors have no conflicts to disclose.

DATA AVAILABILITY

The data that support the findings of this study are available within the article.

REFERENCES

- ¹D. B. DeGraaff and J. K. Eaton, “Reynolds-number scaling of the flat-plate turbulent boundary layer,” *J. Fluid Mech.* **422**, 319–346 (2000).
- ²J. Kim, “Progress in pipe and channel flow turbulence, 1961–2011,” *J. Turbul.* **13**, 1–19 (2012).
- ³M. Lee and R. D. Moser, “Direct numerical simulation of turbulent channel flow up to $Re_\tau \approx 5200$,” *J. Fluid Mech.* **774**, 395–415 (2015).
- ⁴I. Marusic, W. J. Baars, and N. Hutchins, “Scaling of the streamwise turbulence intensity in the context of inner-outer interactions in wall turbulence,” *Phys. Rev. Fluids* **2**, 100502 (2017).
- ⁵X. Chen and K. R. Sreenivasan, “Reynolds number scaling of the peak turbulence intensity in wall flows,” *J. Fluid Mech.* **908**, R3 (2021).
- ⁶A. J. Smits, M. Hultmark, M. Lee, S. Pirozzoli, and X. Wu, “Reynolds stress scaling in the near-wall region of wall-bounded flows,” *J. Fluid Mech.* **926**, A31 (2021).
- ⁷P. A. Monkewitz, “Asymptotics of stream-wise Reynolds stress in wall turbulence,” *J. Fluid Mech.* **931**, A18 (2022).
- ⁸I. Marusic, K. A. Chauhan, V. Kulandaivelu, and N. Hutchins, “Evolution of zero-pressure-gradient boundary layers from different tripping conditions,” *J. Fluid Mech.* **783**, 379–411 (2015).
- ⁹C. E. Willert, J. Soria, M. Stanislas, J. Klinner, O. Amili, M. Eisfelder, C. Cuvier, G. Bellani, T. Fiorini, and A. Talamelli, “Near-wall statistics of a turbulent pipe flow at shear Reynolds numbers up to 40 000,” *J. Fluid Mech.* **826**, R5 (2017).
- ¹⁰M. Samie, I. Marusic, N. Hutchins, M. K. Fu, Y. Fan, M. Hultmark, and A. J. Smits, “Fully resolved measurements of turbulent boundary layer flows up to $Re_\tau = 20000$,” *J. Fluid Mech.* **851**, 391–415 (2018).
- ¹¹A. A. Townsend, *The Structure of Turbulent Shear Flow*, 2nd ed. (Cambridge University Press, Cambridge, 1976).
- ¹²M. Hultmark, M. Vallikivi, S. C. C. Bailey, and A. J. Smits, “Turbulent pipe flow at extreme Reynolds numbers,” *Phys. Rev. Lett.* **108**, 094501 (2012).
- ¹³N. Hutchins, T. B. Nickels, I. Marusic, and M. S. Chong, “Hot-wire spatial resolution issues in wall-bounded turbulence,” *J. Fluid Mech.* **635**, 103–136 (2009).
- ¹⁴M. Hultmark, M. Vallikivi, S. C. C. Bailey, and A. J. Smits, “Logarithmic scaling of turbulence in smooth- and rough-wall pipe flow,” *J. Fluid Mech.* **728**, 376–395 (2013).
- ¹⁵A. J. Smits, J. Monty, M. Hultmark, S. C. C. Bailey, N. Hutchins, and I. Marusic, “Spatial resolution correction for wall-bounded turbulence measurements,” *J. Fluid Mech.* **676**, 41–53 (2011).

- ¹⁶M. Hultmark, S. C. C. Bailey, and A. J. Smits, “Scaling of near-wall turbulence in pipe flow,” *J. Fluid Mech.* **649**, 103–113 (2010).
- ¹⁷N. Furuichi, Y. Terao, Y. Wada, and Y. Tsuji, “Friction factor and mean velocity profile for pipe flow at high Reynolds numbers,” *Phys. Fluids* **27**, 095108 (2015).
- ¹⁸N. Furuichi, H. Sato, Y. Terao, and M. Takamoto, “A new calibration facility for water flowrate at high Reynolds number,” *Flow Meas. Instrum.* **20**, 38–47 (2009).
- ¹⁹N. Kurihara, Y. Terao, S. Nakao, and M. Takamoto, “Development and uncertainty analysis of a laser Doppler velocimeter calibrator for the flow velocity standard,” *Trans. JSME, B* **65**, 3029–3034 (1999) (in Japanese).
- ²⁰N. Kurihara, Y. Terao, S. Nakao, and M. Takamoto, “An uncertainty of laser Doppler velocimeter calibration for air speed standard,” *Trans. JSME, B* **71**, 2100–2107 (2005) (in Japanese).
- ²¹N. Furuichi, Y. Terao, Y. Wada, and Y. Tsuji, “Further experiments for mean velocity profile of pipe flow at high Reynolds number,” *Phys. Fluids* **30**, 055101 (2018).
- ²²F. Durst, J. Jovanović, and J. Sender, “LDA measurements in the near-wall region of a turbulent pipe flow,” *J. Fluid Mech.* **295**, 305–335 (1995).
- ²³J. G. M. Eggels, F. Unger, M. H. Weiss, J. Westerweel, R. J. Adrian, R. Friedrich, and F. T. M. Nieuwstadt, “Fully developed turbulent pipe flow: A comparison between direct numerical simulation and experiment,” *J. Fluid Mech.* **268**, 175–210 (1994).
- ²⁴M. P. Schultz and K. A. Flack, “The rough-wall turbulent boundary layer from the hydraulically smooth to the fully rough regime,” *J. Fluid Mech.* **580**, 381–405 (2007).
- ²⁵F. Durst, M. Fischer, J. Jovanović, and H. Kikura, “Methods to set up and investigate low Reynolds number, fully developed turbulent plane channel flows,” *J. Fluids Eng.* **120**, 496–503 (1998).
- ²⁶M. Fischer, J. Jovanović, and F. Durst, “Reynolds number effects in the near-wall region of turbulent channel flows,” *Phys. Fluids* **13**, 1755–1767 (2001).
- ²⁷M. P. Schultz and K. A. Flack, “Reynolds-number scaling of turbulent channel flow,” *Phys. Fluids* **25**, 025104 (2013).
- ²⁸H.-E. Albrecht, M. Borys, N. Damaschke, and C. Tropea, *Laser Doppler and Phase Doppler Measurement Techniques* (Springer, Berlin/Heidelberg, 2003).
- ²⁹A. Segalini, R. Örlü, P. Schlatter, P. H. Alfredsson, J. D. Ruedi, and A. Talamelli, “A method to estimate turbulence intensity and transverse Taylor microscale in turbulent flows from spatially averaged hot-wire data,” *Exp. Fluids* **51**, 693–700 (2011).
- ³⁰J. Philip, R. Baidya, N. Hutchins, J. P. Monty, and I. Marusic, “Spatial averaging of streamwise and spanwise velocity measurements in wall-bounded turbulence using V- and ×-probes,” *Meas. Sci. Technol.* **24**, 115302 (2013).
- ³¹C. Chin, N. Hutchins, A. S. H. Ooi, and I. Marusic, “Use of direct numerical simulation (DNS) data to investigate spatial resolution issues in measurements of wall-bounded turbulence,” *Meas. Sci. Technol.* **20**, 115401 (2009).
- ³²C. Chin, N. Hutchins, A. Ooi, and I. Marusic, “Spatial resolution correction for hot-wire anemometry in wall turbulence,” *Exp. Fluids* **50**, 1443–1453 (2011).
- ³³P. A. Monkewitz, R. D. Duncan, and H. M. Nagib, “Correcting hot-wire measurements of stream-wise turbulence intensity in boundary layers,” *Phys. Fluids* **22**, 091701 (2010).
- ³⁴Y. Wada, N. Furuichi, and T. Yoshiyuki, “Correction method of measurement volume effects on time-averaged statistics for laser Doppler velocimetry,” *Eur. J. Mech.-B* **91**, 233–233 (2022).
- ³⁵Y. Wada, E. Kusano, N. Furuichi, and Y. Tsuji, “Turbulence intensity profile in high Reynolds number pipe flow,” in 11th International Symposium on Turbulence and Shear Flow Phenomena (TSFP11) Proceeding, 2019.
- ³⁶F. Durst, R. Müller, and A. Naqwi, “Measurement accuracy of semiconductor LDA systems,” *Exp. Fluids* **10**, 125–137 (1990).
- ³⁷C. Chin, J. P. Monty, and A. Ooi, “Reynolds number effects in DNS of pipe flow and comparison with channels and boundary layers,” *Int. J. Heat Fluid Flow* **45**, 33–40 (2014).
- ³⁸S. Pirozzoli, J. Romero, M. Fatica, R. Verzicco, and P. Orlandi, “One-point statistics for turbulent pipe flow up to,” *J. Fluid Mech.* **926**, A28 (2021).
- ³⁹Y. Yamamoto and Y. Tsuji, “Numerical evidence of logarithmic regions in channel flow at $Re_\tau = 8000$,” *Phys. Rev. Fluids* **3**, 012602(R) (2018).
- ⁴⁰J. Ahn, J. H. Lee, J. Lee, J. Kang, and H. J. Sung, “Direct numerical simulation of a 30R long turbulent pipe flow at $Re_\tau = 3008$,” *Phys. Fluids* **27**, 065110 (2015).
- ⁴¹M. A. Miller, B. Estejab, and S. C. C. Bailey, “Evaluation of hot-wire spatial filtering corrections for wall turbulence and correction for end-conduction effects,” *Exp. Fluids* **55**, 1735 (2014).
- ⁴²J. Ahn, J. H. Lee, S. J. Jang, and H. J. Sung, “Direct numerical simulations of fully developed turbulent pipe flows for $Re_\tau = 180, 544$ and 934 ,” *Int. J. Heat Fluid Flow* **44**, 222–228 (2013).
- ⁴³R. Örlü, T. Fiorini, A. Segalini, G. Bellani, A. Talamelli, and P. H. Alfredsson, “Reynolds stress scaling in pipe flow turbulence—First results from CICLoPE,” *Philos. Trans. R. Soc., A* **375**, 20160187 (2017).